BEAM-BEAM EFFECTS

L.R. Evans and J. Gareyte
CERN, Geneva, Switzerland

ABSTRACT

The beam-beam interaction imposes severe limitations on the performance of colliding beam storage rings. In linear colliders the self-pinching effect of the beam-beam force can enhance their perfomance.

1. INTRODUCTION

Particles circulating in a colliding beam storage device experience localised periodic kicks when crossing the opposing beam. As the intensity increases, this beam-beam interaction has a profound effect on the beam dynamics, ultimately limiting the performance of all existing lepton storage rings as well as the SPS hadron collider. It is therefore not surprising that a great deal of experimental, theoretical and computational effort has gone into trying to understand the underlying physics.

For lepton machines, computer simulations have been particularly productive in understanding and predicting machine performance limitations due to this effect. In contrast, in hadron colliders computer simulation is hampered paradoxically by the conservative nature of the beam dynamics and one has to rely more heavily on approximate analytical models based on the theory of nonlinear resonance effects[1-5].

In the near future the first linear collider will be commissioned[6]. Although the beams only pass once through one another, a very strong beam-beam interaction, commonly known as beam disruption, will occur. In contrast with storage rings this disruption has a potentially beneficial effect, strongly focussing both beams and increasing the luminosity by a substantial factor.

2. THE BEAM-BEAM FORCE

We consider first the simplest case of head-on collisions between two round Gaussian bunches of length L with n particles per unit length and with a transverse density distribution

$$\rho(r) = \frac{ne}{2\pi\sigma^2} e^{-r^2/2\sigma^2} .$$

(2.1)

The Lorentz force on a test particle at a radius r is

$$\underline{F} = e(\underline{E} + \underline{v} \times \underline{B}) = e(E_r \pm \beta c B_\phi) \cdot \underline{r} \qquad (2.2)$$

where the negative sign corresponds to a particle in the same bunch and the positive sign to a particle in the other beam, $\underline{r}$ is the unit vector.

The radial electric field E_r and the poloidal magnetic induction B_ϕ can be obtained from Gauss' theorem and Ampère's law respectively.

$$2\pi r E_r = \frac{1}{\epsilon_o} \int_o^r 2\pi r' \rho(r') \, dr'$$

so

$$E_r = \frac{ne}{2\pi r \epsilon_o} (1 - e^{-r^2/2\sigma^2}) , \qquad (2.3)$$

$$2\pi r B_\phi = \mu_o \int_o^r 2\pi r' \beta c \, \rho(r') \, dr'$$

and

$$B_\phi = \frac{ne\mu_o \beta c}{2\pi r} (1 - e^{-r^2/2\sigma^2}) . \qquad (2.4)$$

Then

$$F_r = \frac{ne^2}{2\pi r \epsilon_o} (1 \pm \beta^2) (1 - e^{-r^2/2\sigma^2}) . \qquad (2.5)$$

The angular kick $\Delta x'$ due to the beam-beam interaction is then given by

$$\Delta x' = \frac{Ne}{2\pi \, \epsilon_o \, \beta c \, B\rho} \cdot \frac{1}{x} (1 - e^{-x^2/2\sigma^2}) \qquad (2.6)$$

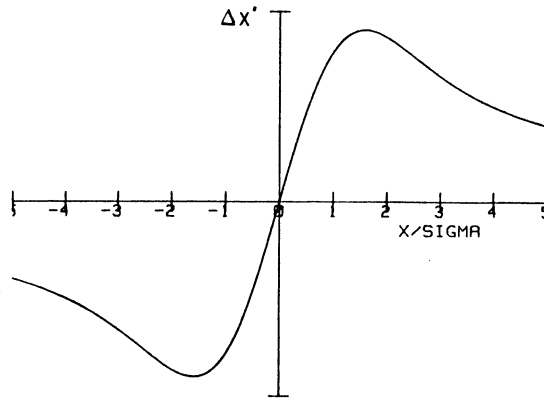where N is the number of particles per bunch and we consider only the plane $y = 0$.

Fig. 1   Beam-beam kick for a round Gaussian beam

For the general case ($\sigma_x \neq \sigma_y$) the beam-beam kick can be obtained by solving Poisson's equation for the generalised electromagnetic potential of an elliptical bunch[7]

$$V(x,y) = \frac{ne}{4\pi\varepsilon_0} \int\limits_0^\infty dt \; \frac{1 - e^{-\left(\frac{x^2}{2\sigma_x^2 + t} + \frac{y^2}{2\sigma_y^2 + t}\right)}}{\sqrt{(2\sigma_x^2 + t)(2\sigma_y^2 + t)}} \quad . \qquad (2.7)$$

The kicks $\Delta x'$ and $\Delta y'$ due to the beam-beam interaction are then

$$\Delta x' = -\frac{\partial V}{\partial x} \quad \text{and} \quad \Delta y' = -\frac{\partial V}{\partial y} \quad .$$

2.1 The Linear Tune Shift

For small amplitude particles, the beam-beam kick is identical to that given by a linear lens of focal length f given by

$$
\begin{aligned}
1/f &= \Delta x'/x \\
&= \frac{Ne}{4\pi\varepsilon_0 \beta c B \rho \sigma^2} \\
&= \frac{Nr_0}{\gamma\sigma^2}
\end{aligned}
\qquad (2.8)
$$

where r_0 is the classical particle radius $r_0 = e^2/(4\pi\varepsilon_0 m_0 c^2)$.

To investigate the perturbation of the lattice functions by this lens we compute the perturbed one-turn transfer matrix

$$
\begin{bmatrix} \cos(\mu + \Delta\mu) & \beta^*\sin(\mu + \Delta\mu) \\ -\frac{1}{\beta^*}\sin(\mu + \Delta\mu) & \cos(\mu + \Delta\mu) \end{bmatrix}
\qquad (2.9)
$$

$$
= \begin{bmatrix} 1 & 0 \\ -\frac{1}{2f} & 1 \end{bmatrix} \cdot \begin{bmatrix} \cos\mu & \beta_0^*\sin\mu \\ -\frac{1}{\beta_0^*}\sin\mu & \cos\mu \end{bmatrix} \cdot \begin{bmatrix} 1 & 0 \\ -\frac{1}{2f} & 1 \end{bmatrix}
$$

where $\mu + \Delta\mu$ and β^* are the perturbed lattice functions.

Then

$$
\begin{aligned}
\cos(\mu + \Delta\mu) &= \cos\mu - \frac{\beta_0^*}{2f}\sin\mu \\
&= \cos\mu - 2\pi\xi\sin\mu
\end{aligned}
\qquad (2.10)
$$

where
$$\xi = \frac{N r_o \beta^*}{4\pi\sigma^2 \gamma} \, .$$
(2.11)

For small $\Delta\mu$,

$$\xi \simeq \frac{\Delta\mu}{2\pi} = \Delta Q_L$$
(2.12)

where ΔQ_L is the linear tune shift due to the beam-beam perturbation.

The corresponding perturbation of the beta function is given by

$$\frac{\Delta\beta^*}{\beta^*_o} = -2\pi\xi \cot \mu \quad .$$
(2.13)

2.2 Stability of Linear Incoherent Motion

In the linear approximation, the motion of a test particle in the presence of the other beam is stable if the absolute value of the trace of the one-turn transfer matrix is less than 2

$$\cos \mu - 2\pi\xi \sin \mu \leq 1$$

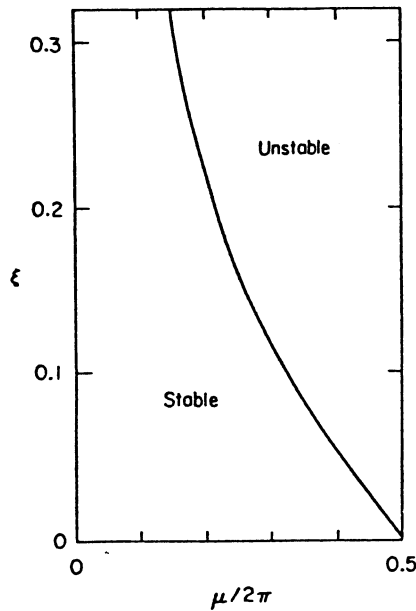$$\xi \leq \frac{1}{2\pi} \cot (\mu/2).$$
(2.14)

Fig. 2   Stability region for a weak beam executing small oscillations. μ is the betatron phase advance between collision points

The experimentally measured limiting beam-beam parameter in lepton machines is of the order of 0.03 to 0.05 and in the SPS hadron collider it is an order of magnitude lower. The linear model clearly predicts a threshold which is much too high.

2.3   Stability of Coherent Motion

For two beams of similar intensity, if one beam is slightly displaced with respect to the other, coherent oscillations are induced which under certain conditions can lead to instability [8,9]. With one bunch per beam, two modes are possible, the 0-mode where both beams move up and down together, and the π -mode where the two beams move in opposite directions. With m bunches per beam, 2 m modes of oscillation are possible. The stability of the system can still be computed by linear matrix theory. For the case of one and three bunches per beam the stability boundary is shown in Fig. 3[9]. Clearly the threshold is substantially reduced compared with the incoherent case, although for the appropriate choice of working point it is still substantially higher than experimentally observed thresholds.
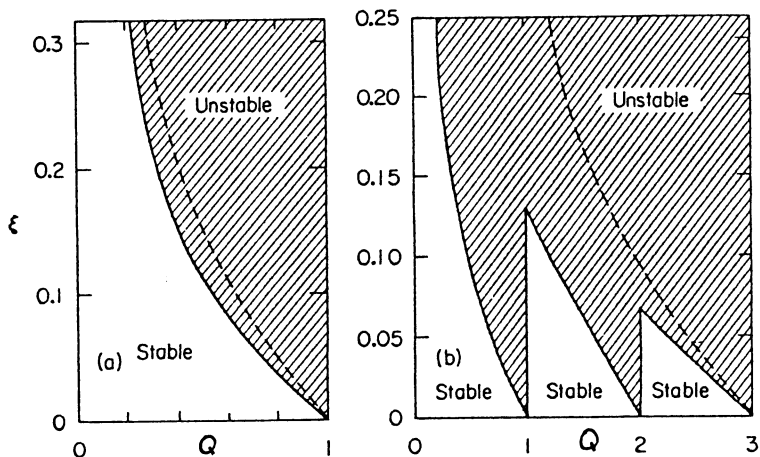

Fig. 3   Stability region for two strong rigid beams executing small center-of-mass oscillations for (a) two colliding bunches and (b) six colliding bunches. The figures are periodic in Q, the total tune of the storage ring; the periods are 1 in (a) and 3 in (b). The dashed lines show the strong-weak stability limit and are reproduced from Fig. 2.

As can be seen from Fig. 1 the beam beam force is intrinsically nonlinear above about 1.5 σ. The nonlinearity has important consequences on the beam dynamics. The effect will be discussed in more detail in Section 5.

2.4 Scaling of the Linear Tune Shift

For the general case of an elliptical beam with Gaussian distribution, the tune shift parameter ξ is given by

$$\xi_{x,y} = \frac{N r_o e}{2\pi\gamma \ (\sigma_x + \sigma_y)} \cdot \frac{\beta^*}{\sigma_{x,y}} \qquad (2.15)$$

where β^* is the value of the beta function at the interaction point. This parameter scales differently with energy for hadron and lepton machines.

In a hadron machine the normalised emittance $(\epsilon\beta\gamma)$ is a conserved quantity. Then putting

$$\sigma^2 = \frac{(\epsilon\beta\gamma) \ \beta^*}{4\gamma}$$

and assuming a round beam $(\sigma_x = \sigma_y)$, then

$$\xi = \frac{N r_p}{\pi(\epsilon\beta\gamma)} \qquad (2.16)$$

which is independent of both γ and of the value of β^* at the crossing point.

For lepton machines the situation is different because the equilibrium beam size scales proportional to γ. The tune shift parameter then has a strong γ^{-3} dependence. Consequently, in a machine like LEP where the beams will be injected at low energy it is vital to separate the beams completely during injection and throughout acceleration. In addition, the beams are normally flat at the collision points so the tune shift parameter also depends on the beta functions at the interaction point.

2.5 Nonlinear Beam-Beam Interaction

In the preceding sections , only the linear part of the beam-beam force was considered. In fact, the beam-beam interaction is an intrinsically nonlinear phenomenon and this nonlinearity gives rise to two effects. Firstly, it introduces a dispersion of the tune with amplitude, the beam-beam tune spread. Secondly, the nonlinear kick together with the localised nature of the interaction drives nonlinear resonances wherever the machine tunes satisfy a relationship of the form

$$mQ_x + nQ_y = \text{Integer}$$

where m and n are even integers for head-on collisions between bunches.

These nonlinear resonances can profoundly influence the topology of the phase space. There is a great deal of evidence, both experimental and from computer simulations, that shows that these resonances play an important rôle in determining the nature of the beam-beam interaction.

In the next two sections, some experimental data from lepton and hadron machines is discussed. The physical manifestation of the phenomenon turns out to be quite different in the two types of machine.

Lepton machines are in some ways both simpler and more complex to understand than hadron machines. The tune spread is normally at least an order of magnitude larger than in hadron machines, so the beams straddle many nonlinear resonances and their synchrotron satellites. However, there is a strong damping mechanism through synchrotron radiation emission to counteract the beam-beam interaction, giving rise to an _equilibrium_ situation. This equilibrium is generally achieved after a few damping times and renders the problem particularly suitable to computer simulation. In the next section some results of computer simulations are discussed and compared with real machine data.

In hadron machines the tune spread is sufficiently small that the beams can be kept clear of low‑order resonances. However, as the experimental data will show, resonances of order 10 or even under some conditions of order 16, have been shown to have a catastrophic effect on beam lifetime at quite modest values of the beam-beam tune shift. There is no, or negligible, radiation damping so an equilibrium situation cannot exist as it does in lepton machines. This makes quantitative predictions using computer simulation difficult, although considerable insight can still be obtained from such simulations. However, for a more complete understanding they must be supplemented by a more detailed analysis of the nature of nonlinear beam-beam resonances.

3. EXPERIMENTAL AND NUMERICAL DATA FROM e^+e^- MACHINES

The most comprehensive compilation known to the authors of data from the world's lepton colliders can be found in Ref. 10. One of the most striking features of this data is shown in Fig. 3 of this reference, reproduced below for convenience.

Figure 4 shows the luminosity versus current observed in seven lepton colliders. The luminosity L is given by

$$L = \frac{I^2}{4\pi M e^2 f \; \sigma_x \sigma_y} \tag{3.1}$$

where f is the revolution frequency, M the number of bunches per beam, I the current per beam (assumed equal in the two beams) and $\sigma_{x,y}$ are the standard deviations of the beam sizes at the crossing point.
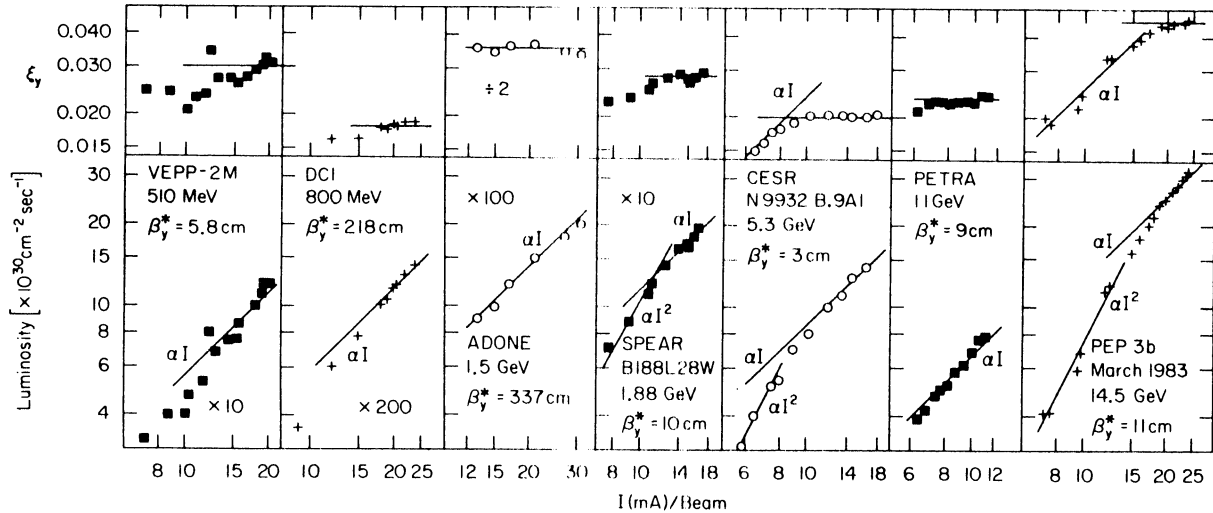

Fig. 4   Luminosity and vertical tune shift parameter versus current for seven electron-positron colliders[10]. Note that the tune shift saturates at some current value above which the luminosity grows linearly.

The behaviour of all seven machines is remarkably similar. At low current, the luminosity increases approximately as the current squared, in agreement with equation (3.1) whereas at high current the luminosity is more proportional to I rather than I^2. Even more striking, the upper plots show the calculated vertical linear beam-beam tune shift parameter ξ_y as a function of current. For a flat beam ($\sigma_y \ll \sigma_x$) ξ_y is given by

$$\xi_y = \frac{I r_o \beta^*}{2\pi M e f \gamma \sigma_x \sigma_y} \tag{3.2}$$

It can be seen that at high current, instead of the linear dependence on current predicted from equation 3.2, the linear tune shift saturates at some value between 0.02 and 0.05. This limiting tune shift is commonly called the 'beam-beam limit'.

In order for σ_y to be constant, the product $\sigma_x \sigma_y$ must increase linearly with current. In practice, the horizontal beam size is observed to change very little and therefore, at the beam-beam limit the vertical beam size must grow linearly with current. This is an important difference between lepton and hadron machines. In $e^+ e^-$ machines, at a given current an equilibrium distribution exists which is a balance

between the heating of the beam due to quantum fluctuations and the beam-beam interaction and the cooling due to synchrotron radiation damping. The beam size has been observed to blow up by as much as a factor of five before the lifetime is affected [11].

The fact that an equilibrium distribution is established in a few damping times (10^3-10^4 turns) makes the beam-beam problem in e^+e^- machines particularly amenable to computer simulation.

3.1 Computer Models of the Beam-Beam Interaction

Computer simulations of the beam-beam interaction have been made in practically all laboratories in which e^+e^- machines exist. The types of simulation can be divided into two main classes, strong-weak and strong-strong.

In strong-weak simulations test particles in the 'weak' beam are tracked through a linear lattice followed by nonlinear beam-beam kicks due to the 'strong' beam which itself is not perturbed by its interaction with the weak beam. Therefore the beam-beam kicks can generally be precalculated and stored in a look-up table with appropriate interpolation. This method is economic in computer time but lacks quantitative predictive power. However, this kind of simulation is useful for studying the beam-beam interaction in, for example, the SPS collider.

More sophisticated simulations treat the strong-strong case, where the changes in beam size and distribution are periodically used to recompute the beam-beam kicks as the calculation proceeds. This kind of simulation can be used to compute the final equilibrium beam size and can quantitatively predict the machine performances (luminosity, beam-beam limit etc.) when the relevant physics is introduced into the problem.

Many different effects can be included in such simulations. In general, as well as the transverse dynamics the longitudinal motion must be taken into account. The synchrotron motion results in a modulation of the arrival time of a particle at the interaction point producing a modulation of the strength of the beam-beam force. This results in the generation of beam-beam synchro-betatron resonances (Section 5) and can sometimes strongly affect the performance[12].

Quantum fluctuations and synchrotron radiation damping are also taken into account. In addition, small errors such as the variation in phase advance between intersection points, small offsets between the beams and spurious dispersion can all have non-negligible effects.

Figure 5 shows one result from a strong-strong simulation at CESR [13], where contours of constant relative luminosity are plotted in the tune space. Areas marked with crosses indicate regions of bad lifetime. These regions are closely correlated to the location of nonlinear resonance lines.
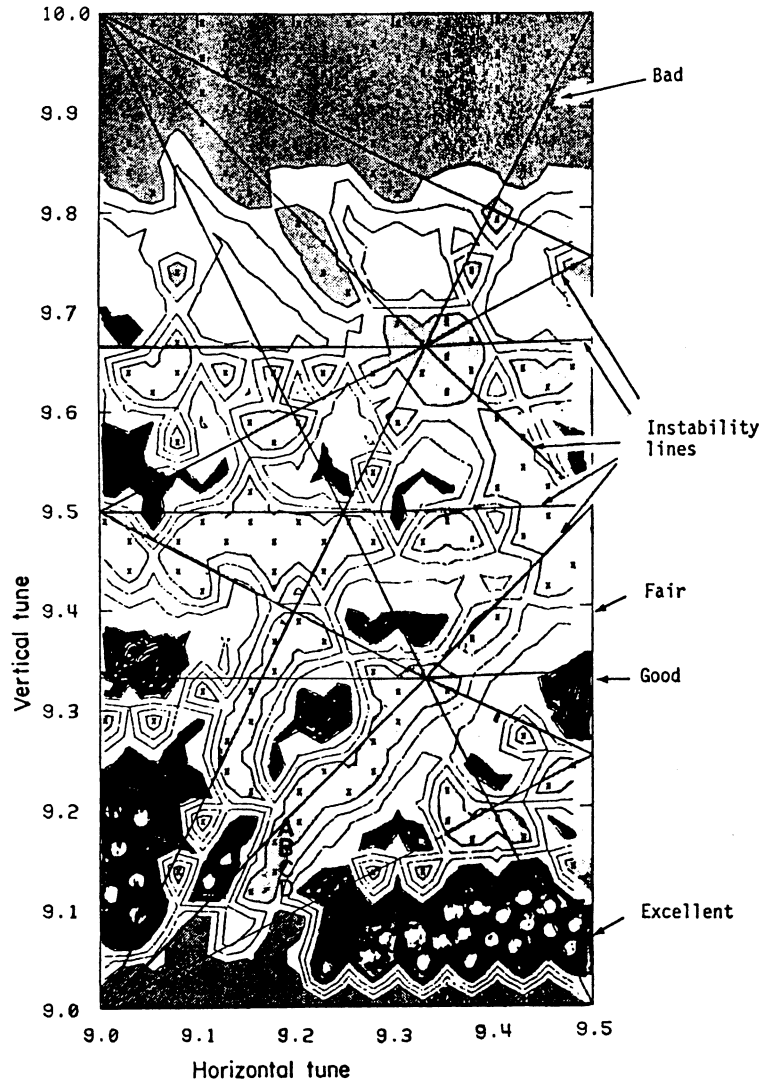

Fig. 5   Beam-beam simulation results for CESR[13]. The contours are at equally spaced relative levels of luminosity. Crosses indicate bad lifetime. The straight lines define the positions of strong nonlinear resonances.

Similar results have been obtained in simulations of LEP [12]. Figure 6 shows the computed luminosity as a function of the vertical tune over a wide range. The regions of low luminosity are again strongly correlated to large azimuthal Fourier harmonics of nonlinear resonances. Note that these simulations have real quantitative predictive value.
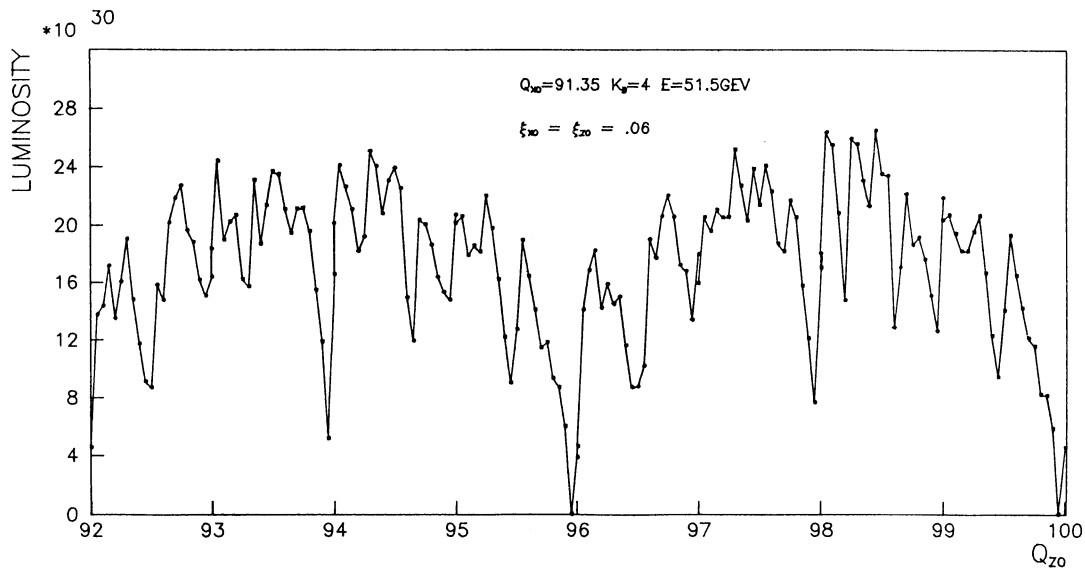
Fig.6   Luminosity (cm⁻².s⁻¹) as a function
         of the vertical tune over a wide range
         computed for LEP[12]. The regions of low
         luminosity coincide with strong nonlinear
         resonances.

Figure 7 shows a similar simulation for Petra[14], where the
equilibrium vertical beam height is plotted as a function of both radial
and vertical tunes. The curves on the left correspond to a perfect
machine. Again, at tune values corresponding to nonlinear resonances the
beam height increases. The situation is much worse when small machine
imperfections are added, in this case small variations in vertical tune
between interaction points and spurious vertical dispersion. The result of
these imperfections is to excite azimuthal Fourier components of the
nonlinear beam-beam force driving resonances which would not normally be
present due to the symmetry of the system. The curves on the right show
how the number and strength of the resonances increases when imperfections
are added.

The predictive value of beam-beam simulations for lepton machines is
illustrated in Fig.   8. These curves were generated using the LEP
simulation code[12] modified for PEP[15]. The top curve corresponds to
the normal PEP working point Q_H = 20.175, Q_V = 25.275. The
experimentally measured luminosity shows good agreement with the
simulation. The program was then used to probe the tune space in search of
a better working point, which was found to be Q_H = 21.275, Q_V =
18.175. When the machine was tuned to this new working point (fig. 8b) the
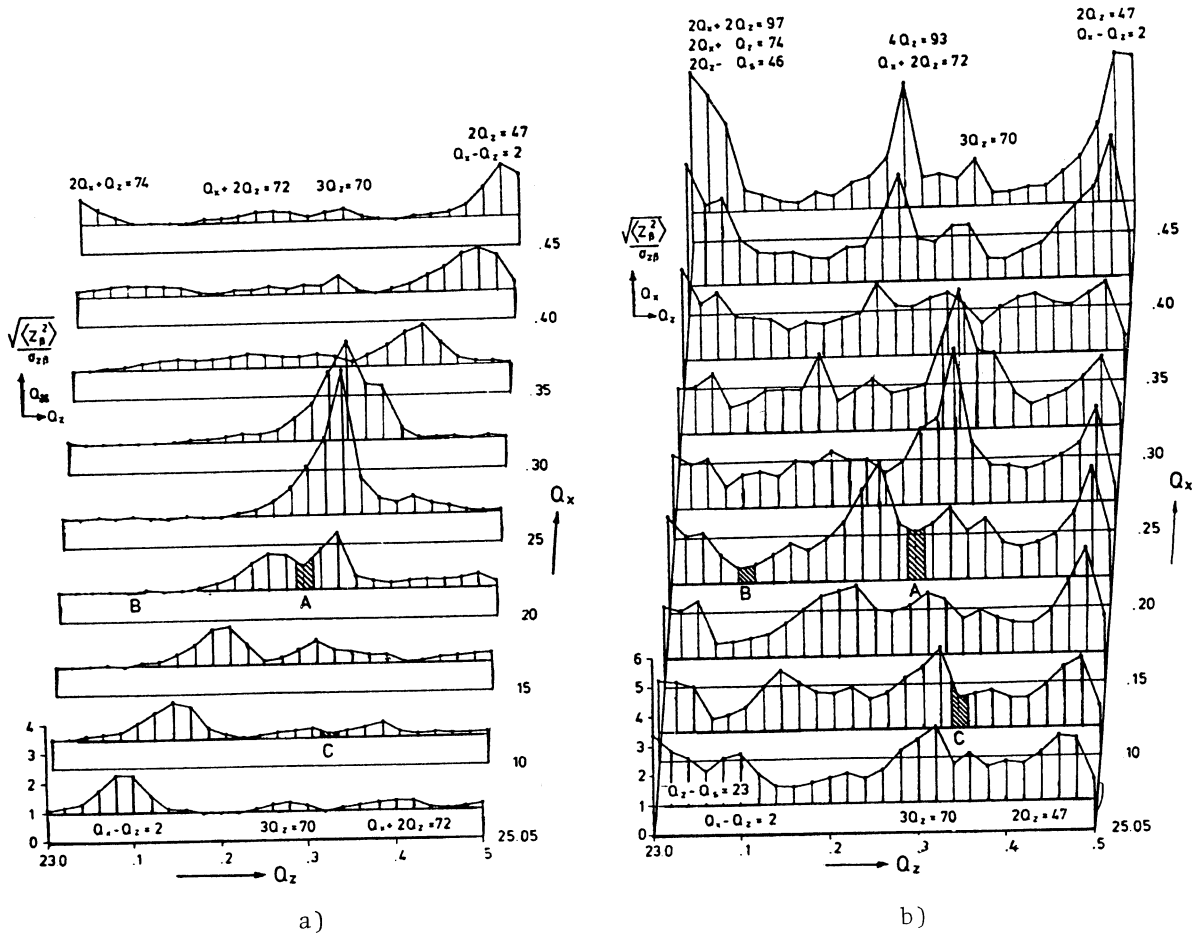luminosity increased as predicted by the simulation, by about 40%.

a)   b)

Fig. 7   Simulated vertical beam height in PETRA[14]
as a function of vertical and horizontal tunes a) without
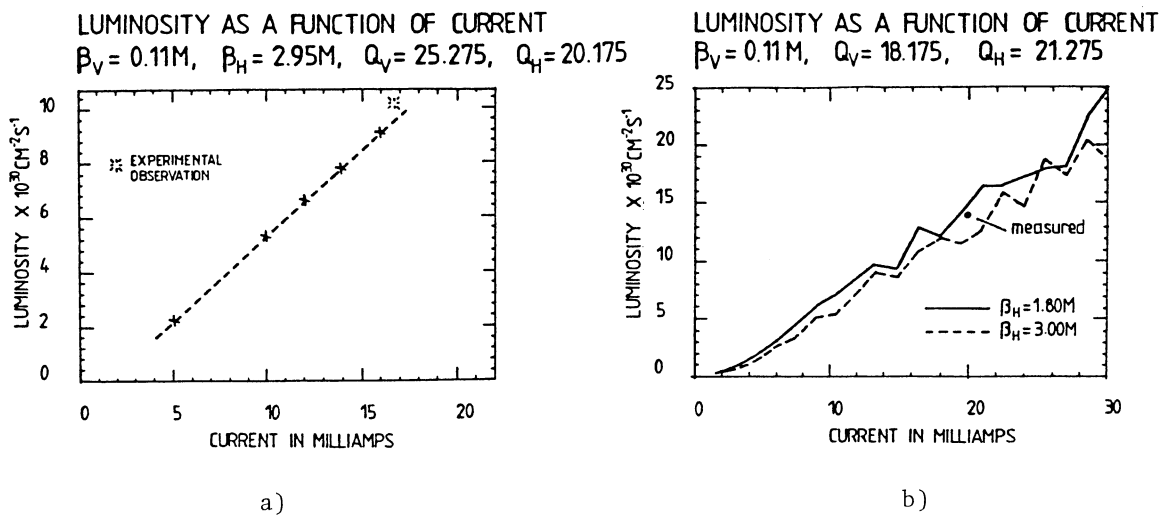machine imperfections and b) with small imperfections.

a)   b)

Fig. 8   Luminosity as a function of current predicted for PEP[15] with the
LEP simulation code[12] and compared with experimental observations.
The better working point b) was predicted by the simulation.

4.   EXPERIMENTAL DATA FROM HADRON MACHINES

At the time of writing, only two hadron colliders have operated, the ISR and the SPS proton-antiproton colliders at CERN, soon to be followed by the Tevatron proton-antiproton collider at Fermilab.

In the ISR the beams were debunched and crossed horizontally at an angle so that in the horizontal plane there was almost no tune shift as a particle was kicked first one way and then the other as it crossed the opposing beam. The only substantial tune shift was in the vertical plane, and this was much smaller $(\sim 4 \times 10^{-4})$ than that obtained in the SPS $(\sim 4 \times 10^{-3})$. The ISR stacked beams on a working line which straddled 7th , 8th and 9th-order resonances (Fig. 9) with very little effect due to the beam-beam interaction.
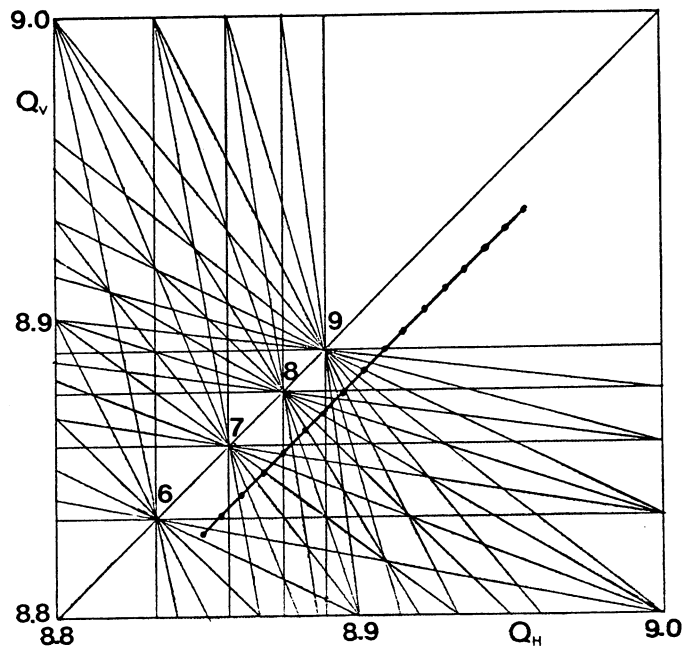

Fig. 9   A typical ISR working line crossing 7th, 8th and 9th-order resonances.

However, the presence of nonlinear resonances could be detected by exciting the beam and measuring the response (beam transfer function)[16]. Figure 10 shows such a measurement on a stack, first with no beam in the other ring and then with successively increasing current. Depletion of the density distribution can be observed at resonant tune values. The amplitude dependence of the tune spread has a stabilizing influence. As the amplitude of a particle increases due to the resonances the tune changes to push the particle off resonance.
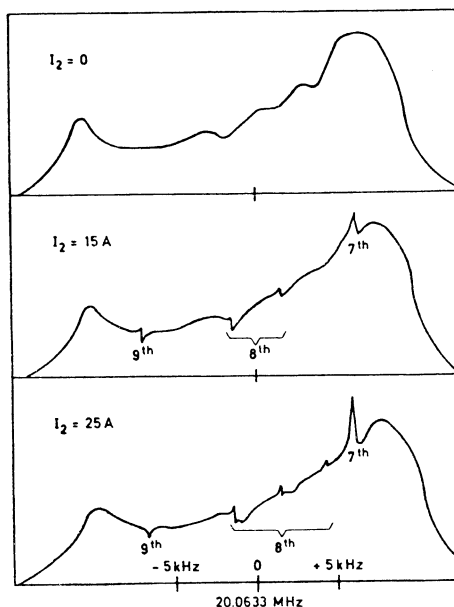
Fig. 10   Vertical beam transfer function measurement
           of the amplitude distribution of beam 1 as
           a function of the current in beam 2,
   showing the beam-beam resonances of order 7
           to 9.

The SPS proton-antiproton collider is more similar to an electron-
positron storage ring. The beams are bunched and collisions are head-on,
giving approximately the same beam-beam tune shifts in the two planes.

Very strong beam-beam effects are observed. Figure 11 shows a scan of
the tune diagram with three proton bunches and a single weak antiproton
bunch (6 crossings per revolution) and with a beam-beam tune shift on the
antiprotons of 3×10^{-3} per crossing[3]. Figure 11a) shows a chart
recorder output of the intensity of one of the proton bunches together
with the antiproton bunch on a very sensitive scale. Figure 11b) shows the
tune diagram between 3rd and 4th-order resonances, where 7th, 10th and
11th-order resonances are indicated.

The intensity decay rate was measured at different positions in the
working diagram, indicated by the lines marked 1,2 etc. The meaning of
these lines is the following. The proton bunch (with which the tune is
measured) has negligible spread and can be considered to occupy a point in
the working diagram indicated by the lower point on each line. The small-
amplitude antiprotons which experience the linear part of the beam-beam
force, are shifted upwards in tune by the total beam-beam spread and
occupy a point at the other end of each line. Large amplitude antiprotons
occupy much of the space between.

The decay rate of the antiprotons is extremely sensitive to the tune, increasing rapidly as the antiprotons touch the 10th-order resonances. In contrast, the proton decay rate under these conditions where proton and antiproton emittances were comparable, was quite insensitive to the tune. In order to have reasonable operating conditions for physics data taking, the tune must be restricted to a very small region of the working diagram corresponding to that of point 1 in the figure. Therefore the beam-beam interaction imposes severe constraints on machine performance.

One way to reduce the tune spread in the beams is to separate the protons and antiprotons at the unwanted collision points (the SPS contains only two experimental areas at adjacent long straight sections Such a separation is possible in the SPS by making global orbit deformations in the opposite sense for protons and antiprotons using a set of four
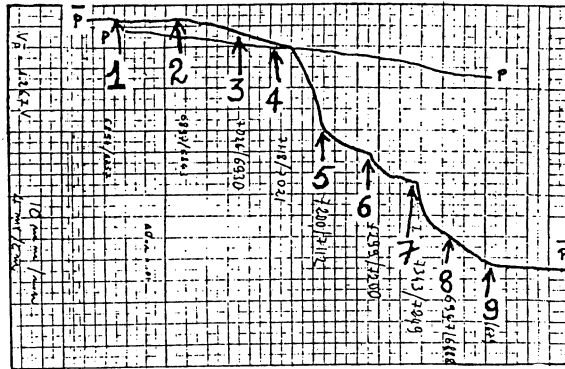
a)
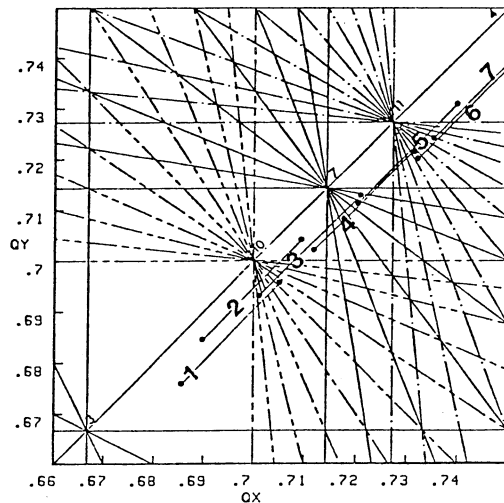
b)

Fig. 11   Scan of the SPS tune space between 3rd and 4th order resonances with a single weak antiproton bunch and three strong proton bunches.

electrostatic deflectors[17]. When the separation is switched on the beam lifetime improves considerably (Fig. 12).
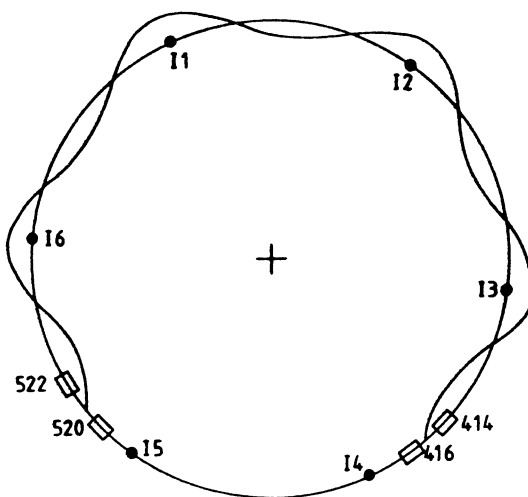

Fig. 12a   Schematic diagram of SPS separation scheme. The proton and antiproton orbits are deformed in opposite directions.
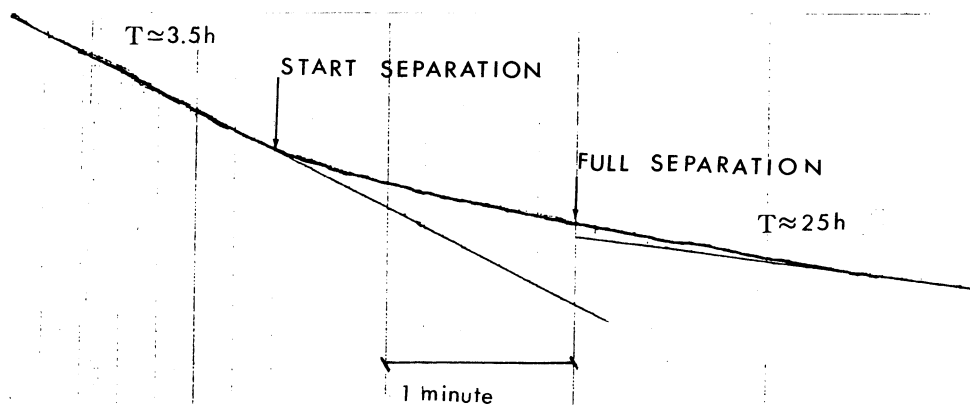

Fig. 12b   Intensity decay of an antiproton bunch as the separation is brought up.

Another important effect observed at the SPS is the self-scraping of large emittance particles when the two beams have unequal emittances. Figure 13 shows the decay rates of three antiproton bunches which were injected with successively bigger emittance. The effect on the decay rates can be easily seen. Antiprotons whose amplitude exceeds the average dimensions of the proton beam are rapidly peeled off and the decay rate is

initially high. As a result the antiproton emittance shrinks during the early phase of storage. The 'dynamic acceptance' of the machine in the presence of the beam-beam interaction is therefore not much more than the strong beam emittance.
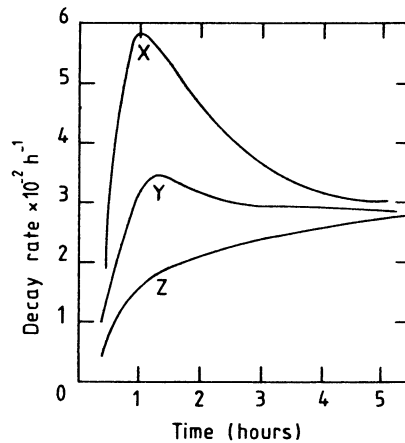

Fig. 13   Decay rates of three antiproton bunches with different emittances. The normalized emittances $E = \epsilon\beta\gamma/\pi$ where $E_x = 17$, $E_y = 15$, $E_z = 12$. The proton emittance $E_p = 16$ and $\xi = .004$.

5.   NONLINEAR BEAM-BEAM RESONANCES

The theory of nonlinear resonances in circular accelerators has been treated elsewhere in these proceedings[4,5]. Before applying the theory to the beam-beam interaction, some of its general features will be briefly reviewed. Detailed derivations are not given here. For these, the reader is referred to Refs. 1-3 and 18-20.

The motion of a test particle in the presence of a nonlinear perturbation is governed by the perturbed Hamiltonian

$$H = H_o + H_1$$

$$= \frac{1}{2}(p_x^2 + p_y^2 + K_x(s)x^2 + Ky(s)y^2) + V(x,y)\delta(s-s_o) \qquad (5.1)$$

where the perturbing potential $V(x,y)$ due to some nonlinear element at azimuthal location $s = s_o$ is considered to be small. The "time" dependence of the nonlinear kick is introduced through the periodic δ-function having period 2π. Note that instead of the time coordinate the azimuthal position s is used.

The general method of solving such a problem[2,18] is first to make two successive canonical transformations, a Courant and Snyder transformation to remove the time dependence of the unperturbed Hamiltonian H_o followed by an action-angle transformation. The periodic δ function is also replaced by a Fourier series expansion.

The next step, for the case of a single multipole is to isolate the 'slowly varying' part of the Hamiltonian when the tune is close to a 'resonant' value $nQ - p \approx 0$. One finally arrives at a 'resonant invariant' (see E.J.N. Wilson's chapter for a detailed derivation) of the form

$$K = (Q - p/n)J + A_n J^{n/2} + B_n J^{n/2} \cos \psi \qquad (5.2)$$

where J is the action variable (Q/2 times the emittance of the orbit) and ψ is the 'slow' phase. The first term in the above expression is the distance of the tune from the resonant tune. The second term corresponds to a variation of tune with amplitude, the nonlinear detuning, and the third term is the 'resonance excitation' term.

The same procedure can be carried out for the case of the beam-beam interaction. However, in this case care must be taken to isolate all the slowly varying terms in the resonant Hamiltonian. These terms come about because the beam-beam force can be decomposed into an infinite series of multipoles. The resonant invariant is of the form

$$K = (Q-p/n) \alpha + \xi u(\alpha) + \xi V_n(\alpha) \cos n\psi \qquad (5.3)$$

where the action variable α has been normalised such that $\alpha = \epsilon\beta/2\sigma^2$.

The tune shift due to the resonances is given by

$$\frac{\partial \psi}{\partial \theta} = \frac{\partial K}{\partial \alpha}$$

$$= (Q-p/n) + \xi u'(\alpha) + \xi V_n'(\alpha) \cos n\psi \quad . \qquad (5.4)$$

Here, $\xi u'(\alpha)$ is the amplitude dependent tune shift, the 'nonlinear detuning' and $\xi V_n'(\alpha)$ is the 'resonance width'. Note that the linear tune shift ξ appears as a scaling parameter.

The functions can be expressed as infinite series[3]:

$$u'(\alpha) = \sum_{m=1}^{\infty} \frac{(-1)^{m-1} (2m)! \, \alpha^{m-1}}{2^{2m-1} (m!)^3} \qquad (5.5)$$

$$V_n'(\alpha) = \sum_{m = n/2}^{\infty} \frac{(-1)^{m-1} \alpha^{m-1} (2m)!}{2^{2m-2} m! (m + \frac{n}{2})! (m - \frac{n}{2})!} \cdot \qquad (5.6)$$

Alternatively they can be expressed in terms of modified Bessel functions[21]:

$$u'(\alpha) = \frac{2}{\alpha} [1 - e^{-\alpha/2} I_0(\alpha/2)]$$

$$V_n'(\alpha) = (-1)^{\frac{n}{2} + 1} \cdot \frac{4}{\alpha} \cdot e^{-\alpha/2} I_{\frac{n}{2}}(\alpha/2) \quad .$$
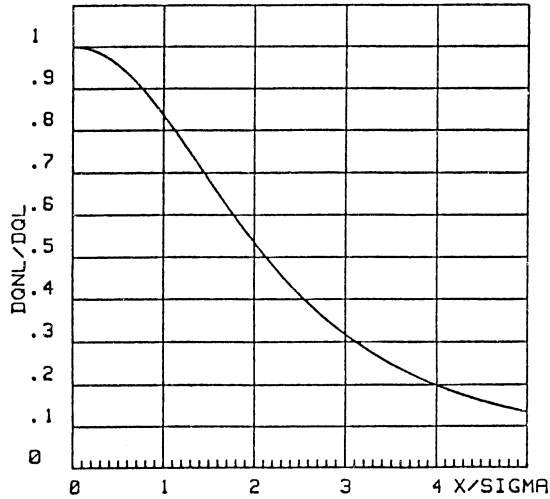

Fig. 14   The nonlinear detuning
function u', with
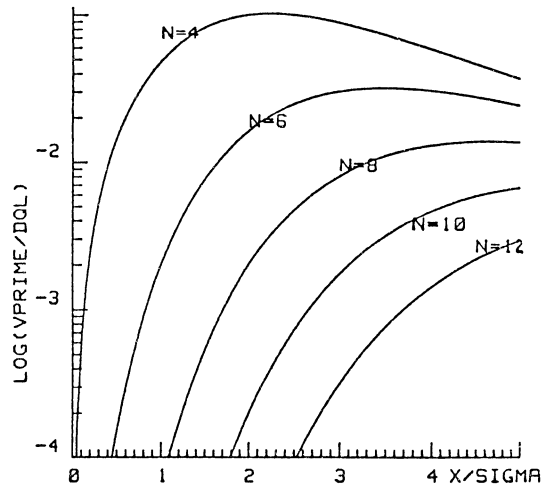$\alpha = x^2/2\sigma^2$

Fig. 15   The resonance width function
for resonances of order 4 to 12

In two dimensions the tune shift and resonances width depends on both horizontal and vertical coordinates. The beam occupies a 'footprint' in the tune space which is shown below for the case of a round beam.
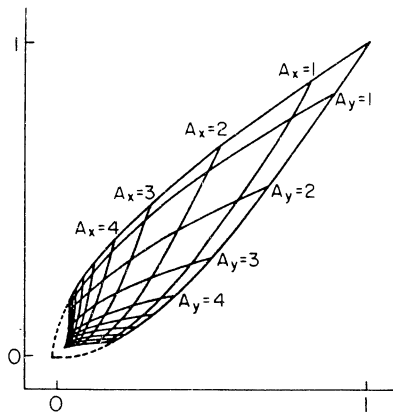

Fig. 16   Nonlinear detuning as a function of x and y
amplitudes A = x/σ for a round beam

Given the resonant invariant 5.3, particle trajectories can be constructed in the 'slow' phase space (α, ψ). When this is done, it is found that the phase space trajectories are stable to a very high value of the linear tune shift. As an example, Fig. 17 shows the trajectories in the vicinity of the 4th-order resonances for a linear tune shift ξ = 0.04. A characteristic island structure can be observed at an amplitude at which the perturbed tune is approximately equal to the resonant tune.
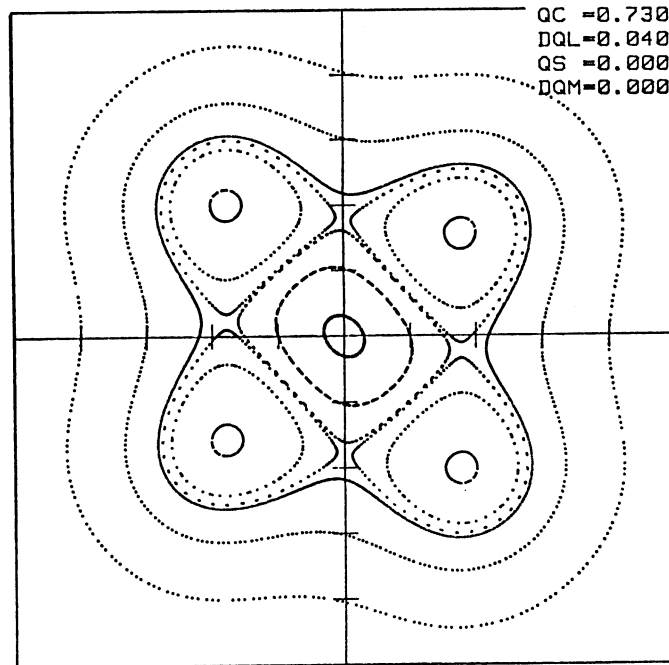

Fig. 17   Phase-space trajectories in the vicinity of
           a 4th-order beam-beam resonances for ξ = 0.04.

5.1. Resonance Overlap

The single-resonance model is clearly inadequate for explaining the beam-beam interaction due to the fact that increasing the beam-beam tune shift increases the destabilizing effect of the resonance excitation and stabilizing effect of the nonlinear detuning proportionately. However, it was first pointed out by Chirikov[22] that the working area is covered by an infinite number of resonance lines for which the tune value is a rational fraction. Although the high-order resonances have narrow width, the fact that there is an infinite number of them may have a significant effect. If they have sufficient width they overlap in the tune space and particle motion will be unstable even if the working area is free of low-order resonances. In Fig. 18 the particular case of the trajectory in the vicinity of a 6th-order beam-beam resonance is shown at the very
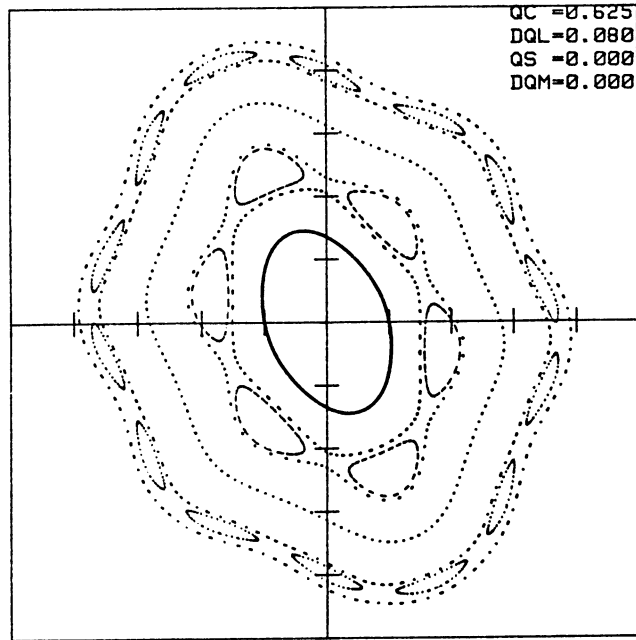
Fig.18   Particle trajectories in the vicinity of a 6th-order beam beam resonance for ξ = 0.08.
At large amplitude the characteristic structure of a 14th order resonance can be observed.

high value of the linear tune shift ξ_m= 0.08. At large amplitude another resonance of order 14 can be observed. If the tune shift increases even further, the two sets of islands will approach each other, and other high-order resonances will appear, finally leading to chaotic motion. However, the linear tune shift required for this phenomenon to occur is still much higher than observed experimentally.

5.2   Synchrobetatron Resonances

The fact that the beam is bunched can have a profound influence on the topology of the transverse phase space. Particles performing energy oscillations can experience a modulation of the transverse tunes due to a number of mechanisms. In lepton machines with short bunches this can arise due to the modulation of the arrival time at the interaction point, resulting in a variation of the strength of the beam-beam kick.   In hadron machines a more important source is due to the small residual chromaticity or a small ripple on the quadrupole power supply. Synchrobetatron resonances are also excited by two beams crossing at an angle [23, 24].

Tune modulation at frequency $Q_m = f_m/f_r$ results in the splitting of a nonlinear resonance $n_1 Q_H + n_2 Q_V = p$ into an infinite number of sidebands

$$n_1 Q_H + n_2 Q_V = p + k \, Q_m.$$

For a one-dimensional resonance of order n, the sidebands are separated by Qm/n and reduced in strength by the factor $J_k(nQ/Qm)$, where $\hat{Q}$ is the amplitude of the modulation. For small Q_m, these sidebands are very close together and can give rise to resonance overlap and stochastic behaviour [20, 25] at a much lower threshold than in the static case, as we shall see below.

5.3   Computer Simulation

Although the resonance invariant (5.3) can be modified to take into account the synchrotron motion, a simple and powerful method of obtaining phase space trajectories is through particle tracking. For a round Gaussian beam the nonlinear beam-beam kick is given by

$$\Delta x' = \frac{8\pi\xi\sigma^2 x}{\beta^* r^2} \; (1 - e^{-r^2/2\sigma^2})$$

$$\Delta y' = \frac{8\pi\xi\sigma^2 y}{\beta^* r^2} \; (1 - e^{-r^2/2\sigma^2})$$

(5.7)

with $r^2 = x^2 + y^2$.

Transforming to new variables $\bar{x} = x/\sigma$, $\bar{x}' = \beta^* x'/\sigma$ we get the position and angle of a particle on turn n + 1 from its coordinates on turn n

$$\bar{X}_{n+1} = \bar{X}_n \cos 2\pi \, Q_{xn} + \bar{X}'_n \sin 2\pi \, Q_{xn}$$

$$\bar{X}'_{n+1} = \bar{X}_n \sin 2\pi \, Q_{xn} + \bar{X}'_n \cos 2\pi \, Q_{xn} - \Delta\bar{X}_{n+1}$$

$$\bar{Y}_{n+1} = \bar{Y}_n \cos 2\pi \, Q_{yn} + \bar{Y}'_n \sin 2\pi \, Q_{yn}$$

$$\bar{Y}'_{n+1} = \bar{Y}_n \sin 2\pi \, Q_{yn} + \bar{Y}'_n \cos 2\pi \, Q_{yn} - \Delta\bar{Y}_{n+1}$$

$$Q_{n+1} = Q_o + \hat{Q} \sin (2\pi \, Q_m \, n) \; .$$

This kind of transformation is called nonlinear mapping. The problem of the stability of such maps is one of considerable current interest in a wide range of disciplines outside the field of particle accelerators.

Now in order to observe the sidebands due to tune modulation the correct timescale for the problem must be chosen. Figure 19 shows a plot of the phase space for an unperturbed tune of 0.7 with a linear beam-beam tune shift $\xi=0.01$, and a tune modulation frequency $Q_m=0.004$. Here the phase-space coordinates of a particle have been plotted <u>once per</u>
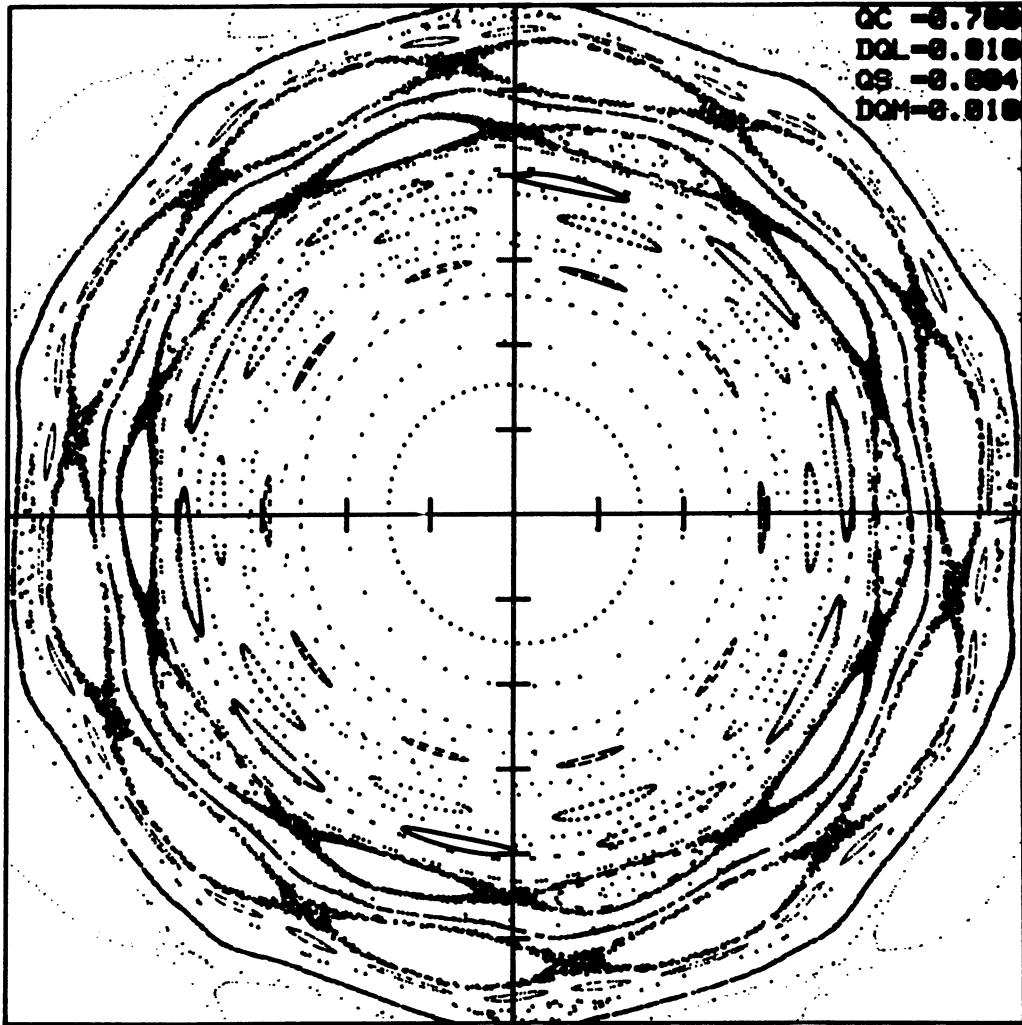
Fig. 19   Phase-space trajectories for an unperturbed
           tune of 0.7 with ξ = 0.01, modulation
           tune Q_m = 0.004 and amplitude Q = 0.01.
           Synchrotron sidebands of a 10th-order
           resonances of order 2 (outer) to 8 are
           visible at amplitudes corresponding to tune
           values 0.7 + $nQ_m/10$. The 7th sideband is
           not visible because the Bessel function
           goes through zero.

synchrotron period, revealing many sidebands of the 10th-order resonance. In this plot, sidebands 2,3,4,5,6 and 8 can be identified. The 7th sideband is not present because the Bessel function $J_7(10\hat{Q}/Q_m)$ goes through zero for the parameters chosen. In this example the islands are well separated and the phase space is stable.

5.4   Stochastic Threshold

The presence of synchrotron satellites enormously increases the density of resonances thereby reducing the Chirikov threshold for

resonance overlap and stochastic behaviour. This threshold can be computed from the resonant invariant by equating the island widths to their separation. The threshold linear tune shift for stochastic behaviour is given by[3, 26]:

$$\xi = \frac{Q_m}{4n} \sqrt{\frac{1}{U''(\alpha) \; V_n(\alpha) \; J_k(n\hat{Q}/Q_m)}} \quad . \quad (5.7)$$

Figure 20 shows the ratio Q_m/ξ as a function of amplitude for the case of a 10th-order resonance.
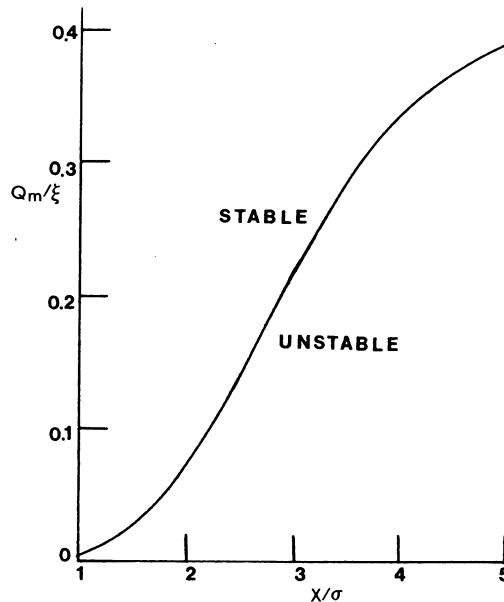

Fig. 20   Stochastic   threshold   as   a   function   of
amplitude   computed   for   a   10th – order
beam–beam resonance.

It is of some interest to compare this analytically computed threshold with the results of a computer simulation. Figure 21 shows the phase space trajectory of a particle with initial amplitude of 4σ in the vicinity of a 10th order resonance and with the very modest beam–beam tune shift parameter $\xi = 1.5 \times 10^{-3}$ and a tune modulation amplitude $\hat{Q}$ of only 4×10^{-4}. The theory predicts that the phase space should be stable when the tune modulation frequency is higher than 5.1×10^{-4}. This agrees quite well with the computer experiment.

The most dominant sources of tune modulation in the SPS collider are due to the unavoidable small residual chromaticity combined with the synchrotron motion and current ripple on the main power supplies. This second source is particularly dangerous because it is at low frequency and a great deal of effort has gone into eliminating it up to a point where
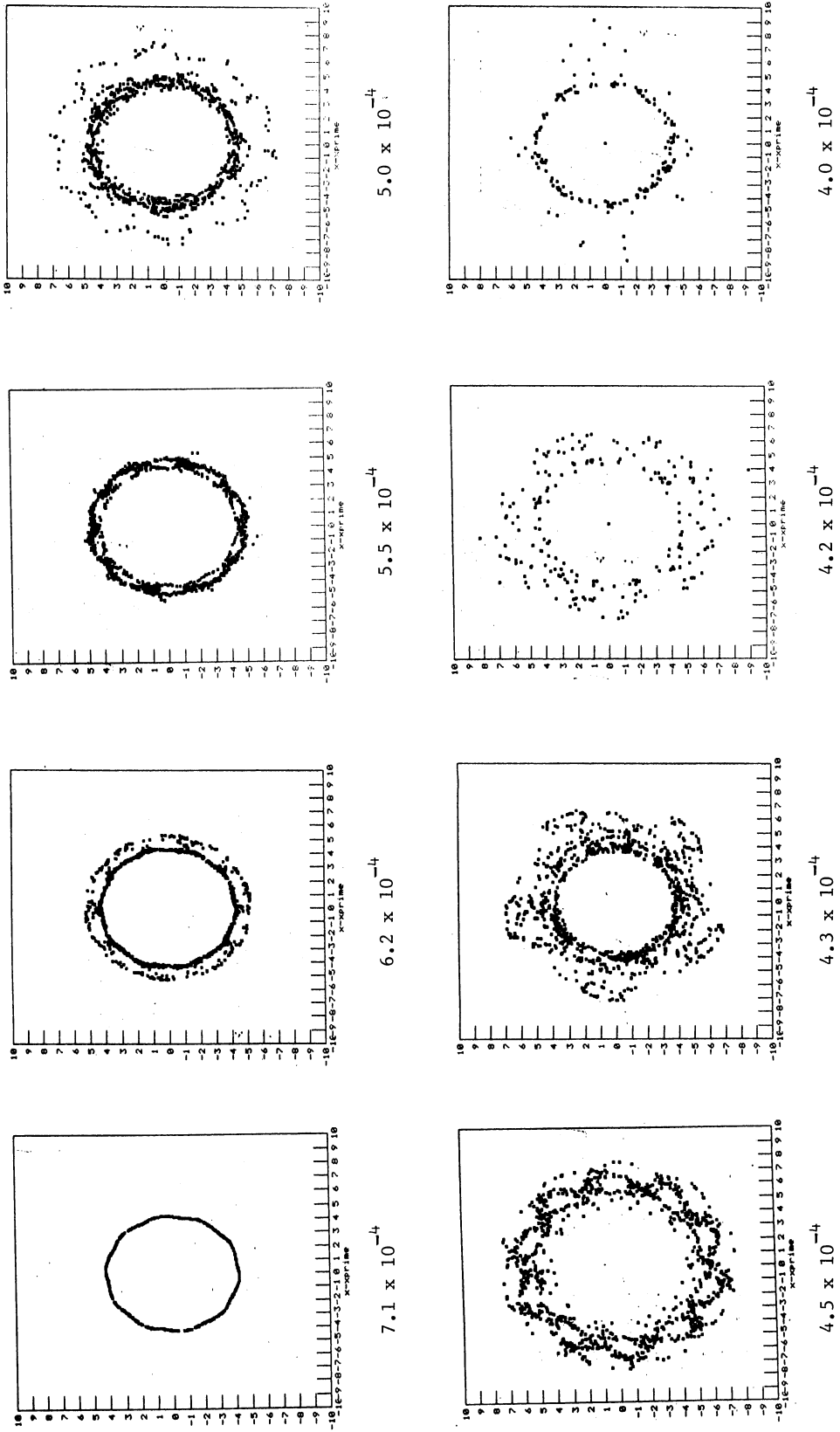
Phase – space trajectories for $\xi = 1.5 \times 10^{-3}$ and $x/\sigma = 4$ as the tune modulation frequency is varied. The stochastic threshold predicted by the analytic theory is at $Q_m = 5.1 \times 10^{-4}$.

Fig. 21

the residual modulation is practically unmeasurable on the sensitive Schottky system used to monitor the machine tunes ($\hat{Q} \underset{\sim}{\sim} 4 \times 10^{-4}$). This frequency dependence of the stochastic threshold may also have important consequences for the very big hadron colliders under consideration at the present time, where the synchrotron frequency is low.

6. BEAM DISRUPTION

This is an extreme form of the beam-beam interaction which will be of considerable importance in single pass linear colliders like the SLC[6]. For two beams of different sign (e^+e^-) the electromagnetic fields due to the beam-beam interaction produce a 'pinch' effect, where both beams are focused. Figure 22 [27] shows a computer simulation of this effect.
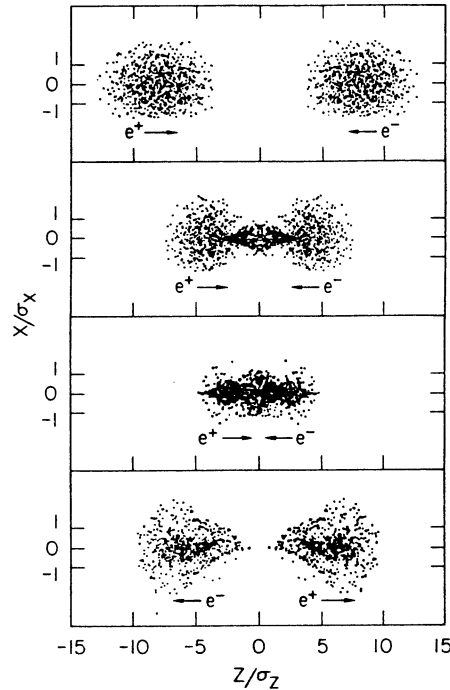

Fig. 22   Pinch effect due to colliding bunches of electrons and positions[26].

The magnitude of the effect is normally parameterized in terms of a disruption parameter D, defined as the ratio of the r.m.s. bunch length to the focal length .

Now
$$\frac{1}{f} = \frac{n r_e}{\sigma_x^2 \, \gamma} \qquad\qquad (6.1)$$

so
$$D = \frac{n r_e \sigma_z}{\gamma \sigma_x^2} \; . \qquad\qquad (6.2)$$

Or, in terms of the beam-beam tune shift ξ

$$D = 4\pi\xi \frac{\sigma_z}{\beta^*} . \tag{6.3}$$

Lepton storage rings generally operate with $\sigma_z/\beta^* \simeq 1$ and the $\xi \simeq 0.05$, giving an effective maximum disruption parameter for a storage ring of the order of 0.6.

In linear colliders it is of interest to operate at a substantially larger value of the disruption parameter because the pinching of the beams can result in a substantially higher luminosity. Figure 23 shows the luminosity gain as a function of D computed for the case of the SLC. For D ~ 5 this simulation predicts a factor of 6 improvement in luminosity. For values of D above about 10 the luminosity gain starts to drop off as the beams pinch each other so strongly as to start to defocus each other within the length of a bunch.
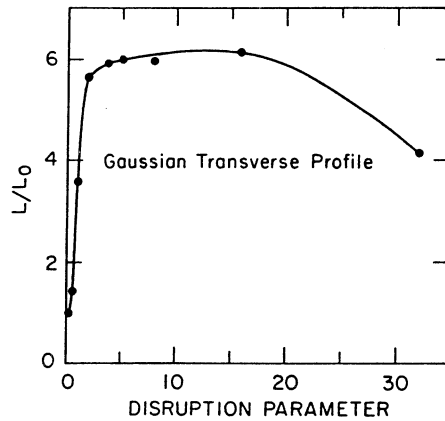

Fig. 23   Luminosity gain in an e^+e^- linear collider as a function of the disruption parameter D[27]. For large D the beams are so strongly disrupted that the luminosity falls off.

7. CONCLUSIONS

Over the last ten years or so, a great deal of effort has gone into trying to understand the details of the beam-beam interaction. For lepton machines, computer simulation has proved to be a powerful tool. Simulation codes have now been developed to the point where they have real predictive value.

For hadron machines the situation is less satisfactory. Although it has not been possible to produce a quantitative predictive model,

analytical calculations supported by computer simulations have shown that synchrobetatron resonances can reduce the threshold for stochastic beam behaviour to a level where the beam-beam interaction has been shown experimentally to play an important role. In future hadron colliders the effect of the low synchrotron tune and the requirement of a non-zero crossing angle at the collision points will have to be given serious consideration.

In linear colliders a new beam-beam effect should manifest itself. Hopefully the SLC will manage to get into a range where the physics of this effect can be investigated experimentally.

<div align="center">*   *   *</div>

REFERENCES

1] A. Schoch, CERN 57-21, (1958).

2] G. Guignard, CERN 78-11, (1978).

3] L.R. Evans, CERN 84-15, p. 319, (1984).

4] J.S. Bell, These Proceedings.

5] E.J.N. Wilson, ibid.

6] SLAC Linear Collider Conceptual Design Report, SLAC-229, (1980).

7] B. Montague, CERN 68-38, (1968).

8] A. Piwinski, Proc. 8th Int. Conf. on High-Energy Accelerators, Geneva, 1971 (CERN, Geneva, 1971), p. 357.

9] A. Chao, AIP Conf. Proceedings, 127, p. 202, (1983).

10] J. Seeman, SLAC-PUB-3825, (1985).

11] A. Piwinski, DESY 83-028, (1983).

12] S. Myers, CERN-ISR/RF/82-06, (1982).

13] S. Peggs and R. Talman, Proc. 11th Int. Conf. on High-Energy Accelerators, Geneva, 1980 (Birkhäuser Basle, 1980), p. 754.

14] A. Piwinski, IEEE Trans. Nucl. Sci., NS-30, p. 2378, (1983).

15] A. Hutton, PEP-Note-375, (1982).

16] G. Guignard, AIP Conf. Proceedings No. 57, p. 69, (1979).

17] L.R. Evans, A. Faugier, R. Schmidt, IEEE Trans. Nucl. Sci. NS-32, p. 2209, (1985).

18] E.D. Courant, R.D. Ruth, W.T. Weng, AIP Conf. Proceedings, 127, p. 294, (1983).

19] A. Jejcic, J. Le Duff, Proc. 8th Int. Conf. on High-Energy Accelerators, p. 354, CERN (1971).

20] J. Tennyson, AIP Conf. Proceedings, 87, p. 345, (1981).

21] M. Month, BNL 19533, (1975).

22] B. Chirikov, Physics Reports, 52, p. 263, (1979).

23] A. Piwinski, IEEE Trans. Nucl. Sci. NS-24, p. 1408, (1977).

24] A. Piwinski, IEEE Trans. Nucl. Sci, NS-32, p. 2240, (1985).

25] E.D. Courant, ISABELLE Tech. Note 163, (1980).

26] S. Peggs, Particle Accelerators, 17, p.11, (1985).

27] R. Hollebeek, Proc. Beam-Beam Interaction Seminar, SLAC-PUB-2624, p 165, (1980).